

## Article

# Tribological Wear Effects of Laser Texture Design on AISI 630 Stainless Steel under Lubricated Conditions

Jorge Salguero <sup>1,\*</sup> , Irene Del Sol <sup>1</sup> , Guzman Dominguez <sup>2</sup> , Moises Batista <sup>1</sup>   
and Juan Manuel Vazquez-Martinez <sup>1</sup> 

<sup>1</sup> Mechanical Engineering and Industrial Design Department, School of Engineering, University of Cadiz, Avenida de la Universidad de Cadiz 10, 11519 Puerto Real, Spain; irene.delsol@uca.es (I.D.S.); moises.batista@uca.es (M.B.); juanmanuel.vazquez@uca.es (J.M.V.-M.)

<sup>2</sup> Mecanizados y Montajes Aeronauticos, Polígono Industrial Salinas Levante, Avdenida Inventor Pedro Cawley 31, 11500 El Puerto de Santa Maria, Spain; guzman.dominguez@mecanizadosymontajes.com

\* Correspondence: jorge.salguero@uca.es

**Abstract:** Surface texturing is used in many applications to control the friction and wear behaviour of mechanical components. The benefits of texture design on the tribological behaviour of conformal surfaces are well known. However, there is a big dependency between the geometrical features of the texture and the texture's performance. In this paper, the effect of laser texturing parameters on textured geometrical features is studied, as well as its role in the tribological behaviour of AISI 630 steel under lubrication and high-contact pressure conditions. The results show a linear impact of the energy density on the surface quality, whereas the scanning speed influences the homogeneity of the sample. Nevertheless, the surface integrity is also affected by the laser parameters, reducing the micro-hardness on the textured area by up to 33%. Friction coefficient average values and stability presented high variations depending on the sample parameters. Finally, the wear mechanisms were analysed, detecting abrasion for the disc and adhesion for the pin.

**Keywords:** LST; AISI 630; tribology; wear; lubricated conditions



**Citation:** Salguero, J.; Sol, I.D.; Dominguez, G.; Batista, M.; Vazquez-Martinez, J.M. Tribological Wear Effects of Laser Texture Design on AISI 630 Stainless Steel under Lubricated Conditions. *Metals* **2022**, *12*, 543. <https://doi.org/10.3390/met12040543>

Academic Editor: Badis Haddag

Received: 25 February 2022

Accepted: 19 March 2022

Published: 23 March 2022

**Publisher's Note:** MDPI stays neutral with regard to jurisdictional claims in published maps and institutional affiliations.



**Copyright:** © 2022 by the authors. Licensee MDPI, Basel, Switzerland. This article is an open access article distributed under the terms and conditions of the Creative Commons Attribution (CC BY) license (<https://creativecommons.org/licenses/by/4.0/>).

## 1. Introduction

Friction and wear are very complex phenomena due to their dependency on micro-geometrical aspects of the surface. Studied since the 18th century, the first attempt to establish friction models resulted in the three classical laws of friction, developed by Amontons and Coulomb [1,2]. In the middle of the 20th century, Bowden and Tabor developed a new model of friction, which states that friction and wear origins are the result of interaction between the surface's asperities [3–5]. Currently, nanoscale and atomic interaction are also considered to characterize and create friction models [6–8].

Friction and wear behavior are highly related to the surfaces of the contact pair. These surfaces can be designed according to their future application. In fact, high-roughness surface designs can be useful for the reduction in friction as well as its increase. In this field, textured surfaces are presented as a suitable solution for friction behavior modification.

Textured surfaces have different behaviors compared with smooth surfaces. The textures reduce the contact area, allowing abrasive particles (from the environment or from wear debris) to become trapped. Similarly, they can act as lubricant reservoirs, improving the load-carrying capacity of the lubricant film due to a cavitation lift force [9–14]. However, texturing decreases the fatigue life of the textured components [15].

In the surface modification field, Laser Surface Texturing (LST) is a technique that has increased in popularity over the last few years. It consists of engraving by machining a pattern on the surface using a laser beam. It has been employed in many mechanical components, such hydrodynamic bearings, mechanical seals, piston rings, cylinders, and cutting-tools, etc. [9,16,17].

LST has many advantages compared with other texturing techniques, such as EBM [18], milling [19], EDM [20], ECM [21] or the geometrical features that can be achieved through additive manufacturing processes [22]. Laser machining is flexible, fast, precise, and reliable. Unlike conventional machining processes, it does not require cutting fluids, and no expendable material is necessary. Thus, LST can be considered as a sustainable manufacturing process, whose only disadvantage is the requirement of a high initial investment [23–26].

LST has been widely employed on the tribological optimization of conformal surfaces under lubrication [27,28]. The characteristics of such surfaces favor the development of a hydrodynamic lubrication regime due to the lower contact pressures [29].

Many authors have researched the influence of the micro-geometrical properties of the textured surface. Dimple-shaped textures, without sharp corners in the sliding direction, have been reported as good choices for reducing the friction coefficient of both hydrodynamic and boundary lubrications [30–32]. The density of the textures plays a crucial role. In high-density textures, the contact area decreases and the friction coefficient and wear increase, as a result of the dispersion of the fluid film. However, high-density textures trap more abrasive particles and store more lubricant, so an optimal texture density (depending on contact, sliding, and materials properties) can be found [33–36].

The size and depth of textures have also been studied. Deep textures lead to the formation of a vortex inside them, diminishing the film thickness and their load-carrying capacity. However, deep textures can store more abrasive particles. A very shallow texture pattern diminishes the overall effect of the textures [37–40], whereas deep textures lead to an increase in the stick–slip phenomenon, due to a decrease in the surface stiffness [41]. Thus, deep textures favor the stick–slip phenomenon, characterized by an oscillation of the friction coefficient between static and dynamic values in the steady-state regime [3]. Therefore, optimal texture size and depth depend on different factors, such as material, lubricant, and contact properties.

Additionally, the behavior of non-conformal contacts (bearing geometries that fail to conform to one another, i.e., ball and rolling elements in bearings, cams, and gears) is different from that of conformal contacts (bearing geometries that have a high degree of conformity, i.e., where one surface fits relatively snugly into the other). It has been reported that textures may act as a barrier to sliding if the contact area is smaller than the textures, leading to an increase in the interaction between the surfaces, and resulting in a stress concentration that can disperse the fluid film [42,43]. In addition, non-conformal contacts favor a boundary lubrication regime [29].

Surface texturing may impact the wettability of a surface, i.e., the capacity to retain liquids. This property depends on the micro geometrical, physical and chemical properties of the surface and the fluid. There are two models which characterize the influence of these factors on wettability: the Wenzel and the Cassie-Baxter models [44–48]. The surface modification induced by the texturing process is expected to modify the wettability of the surface and its behavior toward a lubricated sliding. Many authors have reported that laser texturing is able to change the behavior of a surface from hydrophobic to hydrophilic, and vice versa [49–52].

Finally, AISI 630 is one of the most popular and most commonly used stainless chromium-nickel alloy steels, with a copper additive and precipitation hardened with a martensitic structure. It is characterized by having a high corrosion resistance while maintaining high strength properties, including hardness. It can operate in the temperature range from  $-29\text{ }^{\circ}\text{C}$  to  $343\text{ }^{\circ}\text{C}$ , while retaining relatively good properties. Due to its excellent properties in a wide range of temperatures, it is used in critical components in the aerospace industry (bushings, turbine blades, couplings, drive shafts, and landing gears, etc.). However, although it is used in applications in contact with other elements, the possible improvement of tribological performance by laser texturing has not been studied in the literature.

In this paper, a study of the influence of a laser is presented as a non-conventional machining method to texture AISI 630 stainless steel. Different energy densities have been applied for a constant texture geometry, characterizing its behavior with a tribological pin-on-disc test and the effect of the laser beam on the microstructure across micro-hardness and microscopy techniques.

## 2. Materials and Methods

The experimental methodology consists of three main phases, including specimen preparation, tribological pin-on-disc tests, and specimen characterization. All the tests were repeated at least 3 times.

### 2.1. Specimen Preparation

AISI 630 discs with 40 mm diameter and 5 mm thickness were cut using wire electro-discharge machining (WEDM) from a bar. The discs were grinded and polished by using #800 grit and #1200 grit SiC papers, until reaching an average roughness  $R_a < 0.8 \mu\text{m}$  [53]. AISI 630 composition is shown in Table 1.

**Table 1.** AISI 630 composition (wt%) [54].

C	Si	Mn	P	S	Cr	Ni	Cu	Nb + Ta	Fe
$\leq 0.07$	$\leq 1$	$\leq 1$	$\leq 0.04$	$\leq 0.03$	15–17.5	3–5	3–5	0.15–0.45	rest

Laser texturing was performed under room air atmosphere, using a commercial marking machine (ROFIN-SINAR Technologies Inc., Plymouth, MI, USA) based on the Ytterbium-fiber infrared laser system with an  $\lambda = 1070 \pm 5 \text{ nm}$  wavelength, and a pulse duration of  $\tau = 100 \text{ ns}$ . The texturing process was developed through bidirectional parallel lines with a 0.1 mm distance between the irradiated tracks, using a laser spot with 60  $\mu\text{m}$  of focal diameter.

Seven different treatments were designed to texture the AISI 630 specimen's surface, divided into two sets of laser parameters (Table 2). The first one studied the surface of the sample with a scanning speed ( $V_s$ ) ranging from 10 to 200 mm/s at a fixed energy density of pulses ( $E_d$ ) of 35.37 J/cm<sup>2</sup>. The second set analysed the effect of  $E_d$  in a range between 5.89 and 35.37 J/cm<sup>2</sup> at a  $V_s = 10 \text{ mm/s}$ . Energy density of pulses ( $E_d$ ) was calculated with Equation (1).

$$E_d \left[ \frac{\text{J}}{\text{cm}^2} \right] = \frac{E_t[\text{J}]}{A_{\text{spot}}[\text{cm}^2]} = \frac{P[\text{W}]}{f[\text{Hz}] A_{\text{spot}}[\text{cm}^2]} \quad (1)$$

where  $E_t$  is the pulse energy calculated from power ( $P$ ) and frequency ( $f$ ), and  $A_{\text{spot}}$  is the area of the laser spot.

**Table 2.** Laser texturing parameters.

$E_d$ (J/cm <sup>2</sup> )	5.89	11.79	14.68	35.37
$V_s$ (mm/s)	10	50	100	200

Results were compared with an untextured sample.

Once textured, micro geometrical characteristics have been evaluated in terms of arithmetical mean roughness value ( $R_a$ ), greatest height of the roughness profile ( $R_z$ ), and mean peak width ( $R_{Sm}$ ). From the extracted profiles, texture depth has also been measured. For this purpose, a Mahr Perthometer Concept PGK120 profilometer (Mahr technology, Göttingen, Germany) was used, following the UNE-EN ISO 4288:1999 standard [55]. Additionally, an Alicona Infinite Focus G5+ (Bruker, Germany) variable focus microscope was used to evaluate the surface roughness parameters, as the developed interfacial area ratio ( $S_{dr}$ ) and the arithmetical mean height ( $S_a$ ).  $S_{dr}$  is expressed as the percentage of the definition area's additional surface area contributed to by the texture as compared with

the planar definition area, whereas Sa is the extension of Ra to a surface. It expresses, as an absolute value, the difference in height of each point compared with the arithmetical mean of the surface.

## 2.2. Tribological Tests

Tribological test have been carried out on textured and non-textured AISI 630 discs with a MT/60/Ni pin-on-disc tribometer (Microtest, Madrid, Spain). The discs were the AISI 630 specimens, whereas tungsten carbide (WC-Co) balls, with a diameter of 3 mm, were used as pins. The tests were performed using a linear speed of 0.67 m/s and a normal load of 5 N, resulting in a contact pressure of 1.5 GPa calculated from the classical equations described as Equations (2)–(4) for hertzian contacts (2).

$$P_{max} = 1.5 \cdot \left( \frac{L}{\pi a^2} \right) \quad (2)$$

where  $P_{max}$  is the maximum pressure between the ball and the surface,  $L$  is the load of the sliding test (N), and  $a$  can be calculated following expression (2).

$$a = \sqrt[3]{\frac{3}{8} \sqrt[3]{LdC}} \quad (3)$$

where  $d$  is the diameter of the ball used as a pin, and  $C$  is calculated following expression (3).

$$C = \frac{1 - \nu_1^2}{E_1} + \frac{1 - \nu_2^2}{E_2} \quad (4)$$

where  $\nu$  is the Poisson modulus and  $E$  is the Young modulus for WC-Co and AISI 630, respectively.

The sliding length was 250 m. The evolution of the friction coefficient (CoF) was recorded online during the tests. All tests were carried out in the presence of lubricant, by adding at the start of the test 5  $\mu$ L Renolin MR 3 VG 10, a mineral oil widely applied to lubricate mechanical contacts.

## 2.3. Tribological Wear Characterisation

In order to analyse the morphology, the depth of the textures, and the generated wear track, a cross section of the tested specimens was obtained by WEDM processes. After the WEDM cutting process, all the specimens were ground and polished with #800 grit, #1200 grit, and #4000 grit SiC papers, and the cross-section was observed through metallographic microscopy techniques, using an Epiphot 200 microscopy (Nikon, Japan). In addition, the appearance of microstructural modifications induced by the heat generated during the laser process were examined by a chemical etching of the cross sections by a Fry reagent.

Finally, surface micro-hardness was measured using a Shimadzu HMV micro-hardness tester (Shimadzu, Japan). The Vickers method was used with a load of 0.24 N and 10 s time. Six micro-hardness measurements were taken on each specimen at different distances from the textured area to the bulk material.

## 3. Results and Discussions

### 3.1. Surface Geometry Characterization

The combination of laser processing parameters successfully provided different texture characteristics. LST parameters have an impact on the laser track morphology and size. As is shown in Figure 1a, the depth of the irradiated track is highly influenced by the Ed, showing an exponential increase in the initial values. However, the effect of the Vs does not induce a linear trend, instead providing a peak value for 50 mm/s, as shown in Figure 1b.

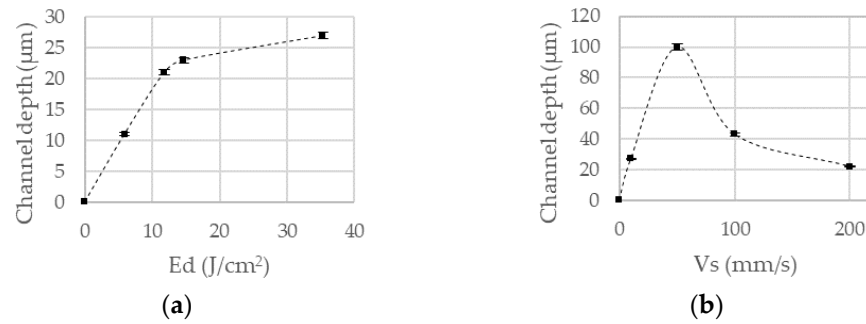


**Figure 1.** Channel depth: (a) For different  $E_d$  at  $V_s = 10$  mm/s; (b) For different  $V_s$  at  $E_d = 35.37$  J/cm<sup>2</sup>.

This surface modification may also be measured using roughness parameters. The parameters evaluated for the textured specimens are shown in Figure 2, where the standard deviation of the results is lower than 2%, which is difficult to be appreciated in the figure.

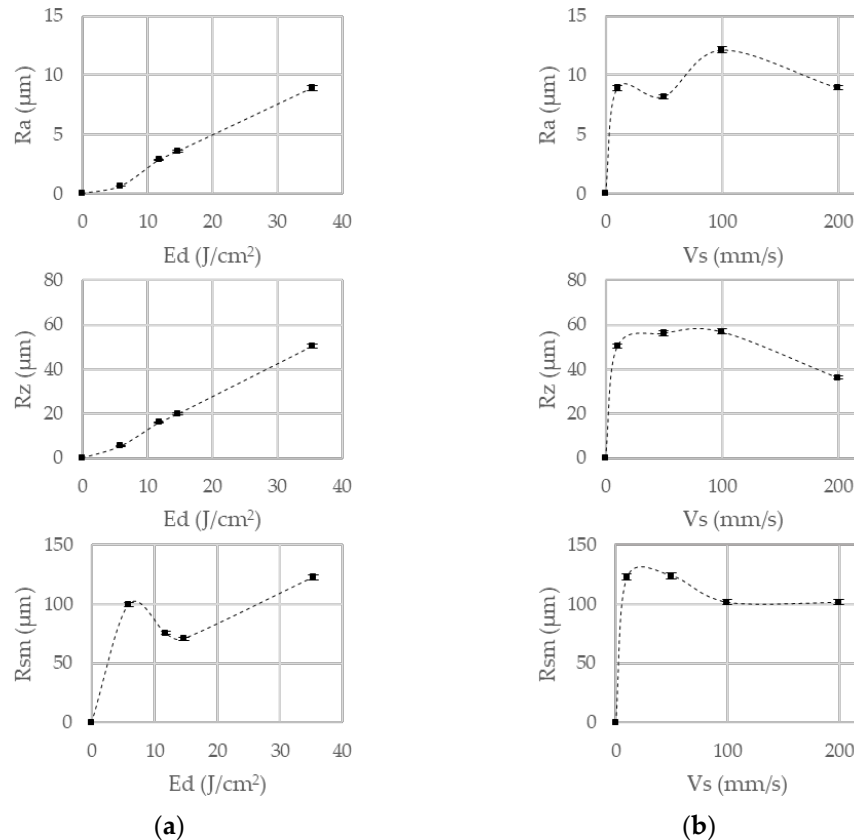


**Figure 2.** Profile Roughness parameters: (a) At different  $E_d$  at  $V_s = 10$  mm/s; (b) At different  $V_s$  at  $E_d = 35.37$  J/cm<sup>2</sup>.

The use of specific combinations of laser processing parameters results in specific variations of the size and shape of the laser tracks. However, the highly complex phenomena that take place in the cooling process after the irradiation process, may cause small variations of the texture characteristics that affect the roughness behavior of the surface.

Ra and Rz follow a linear trend for the  $E_d$  increase due to the higher amount of energy received by the surface. This is caused by a higher material removal rate obtained with high  $E_d$ . As the scanning speed increases, under the same energy density, a fluctuation in roughness around  $10 \mu\text{m}$  is observed, with a peak for  $100$  mm/s. For the RSm values, lower scanning speed values result in the increase in the width of the irradiated tracks. RSm decreases with medium values of  $E_d$ , which is related to narrower channels. This reduction may be produced by the burrs formed on the channel side. These burrs appear due to

the solidification of the removed material at the edges, creating smooth peaks and valleys that reduce the average width of the textured pattern. However,  $V_s$  does not seem to have an impact on this parameter, obtaining  $R_{Sm}$  results within 20% range. As shown in the Figure 2b, the stabilization to 0.1 mm width of tracks was reached for laser treatments where the laser beam does not remain on the same area of the surface for long ( $V_s \geq 100$  mm/s).

These profile data are homogeneous all over the textures as is shown for surface roughness parameters (Figure 3) and textures mapping (Figure 4).

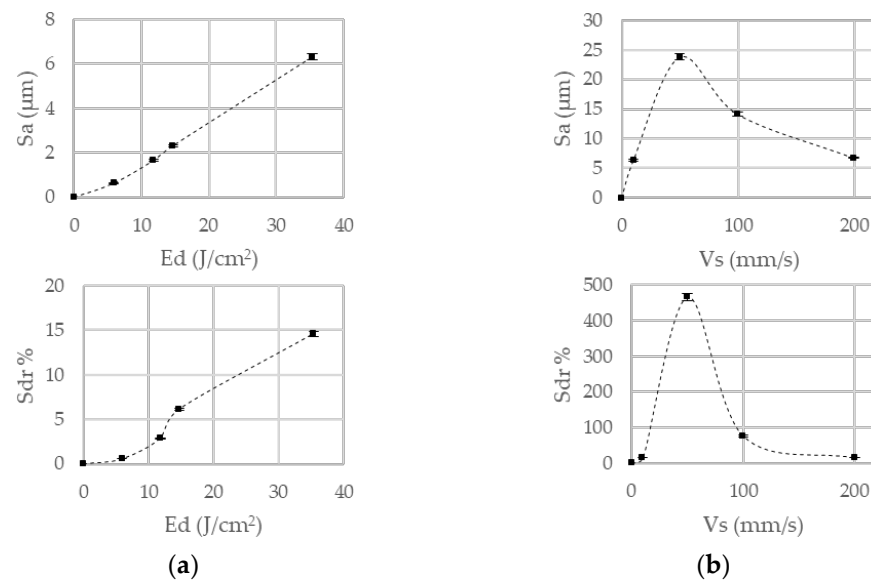


**Figure 3.** Surface roughness parameters: (a) At different  $E_d$  at fixed  $V_s = 10$  mm/s; (b) At different  $V_s$  at fixed  $E_d = 35.37$   $\text{J}/\text{cm}^2$ .

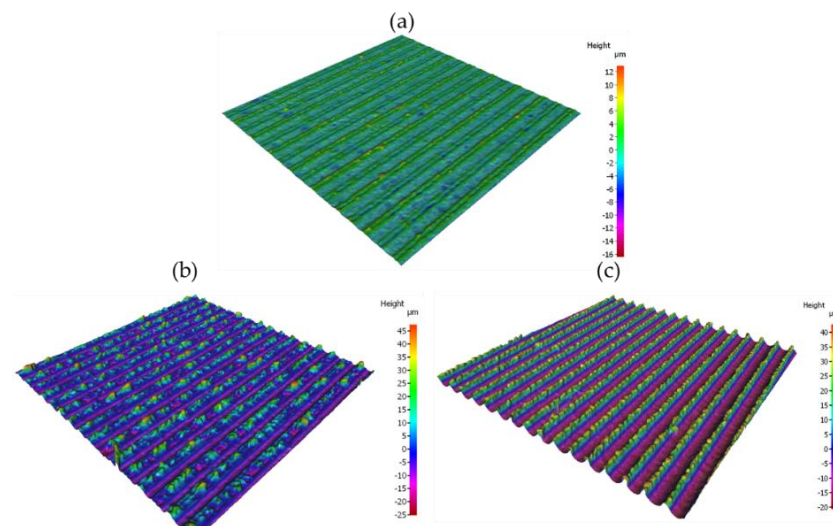


**Figure 4.** Surface topography for samples textured: (a)  $E_d = 11.79$   $\text{J}/\text{cm}^2$  and  $V_s = 10$  mm/s; (b)  $E_d = 35.37$   $\text{J}/\text{cm}^2$  and  $V_s = 10$  mm/s; (c)  $E_d = 35.37$   $\text{J}/\text{cm}^2$  and  $V_s = 100$  mm/s.

As for profile roughness, both  $S_a$  and  $S_{dr}$  follow a linear trend, increasing with  $E_d$ . Nevertheless, the impact of  $V_s$  on  $S_a$  is considerably higher, increasing its value up to  $23.77$   $\mu\text{m}$ . It is up to 75% higher than the maximum value obtained for  $E_d = 35.37$   $\text{J}/\text{cm}^2$  and  $V_s = 10$  mm/s. The results are consistent with the channel depth presented in Figure 1. Similarly, the superficial area is increased by these parameters which may impact the friction coefficient and wear rate. These results enhance the homogeneity of the texture samples, as a result of the selected pattern.

Scanning speed of the beam is highly related to the depth of the laser tracks, as are the Sa values. Under this consideration, the unexpected behavior of the low Sa and Sdr value from the  $35.37 \text{ J/cm}^2$  and  $10 \text{ mm/s}$  specimen is mainly due to a phenomenon that affects the external area of the irradiated track. This effect is caused by the solidification of the vaporized debris on the surface, which in turn reduces the roughness of the textures [28,52], as shown in Figure 5.

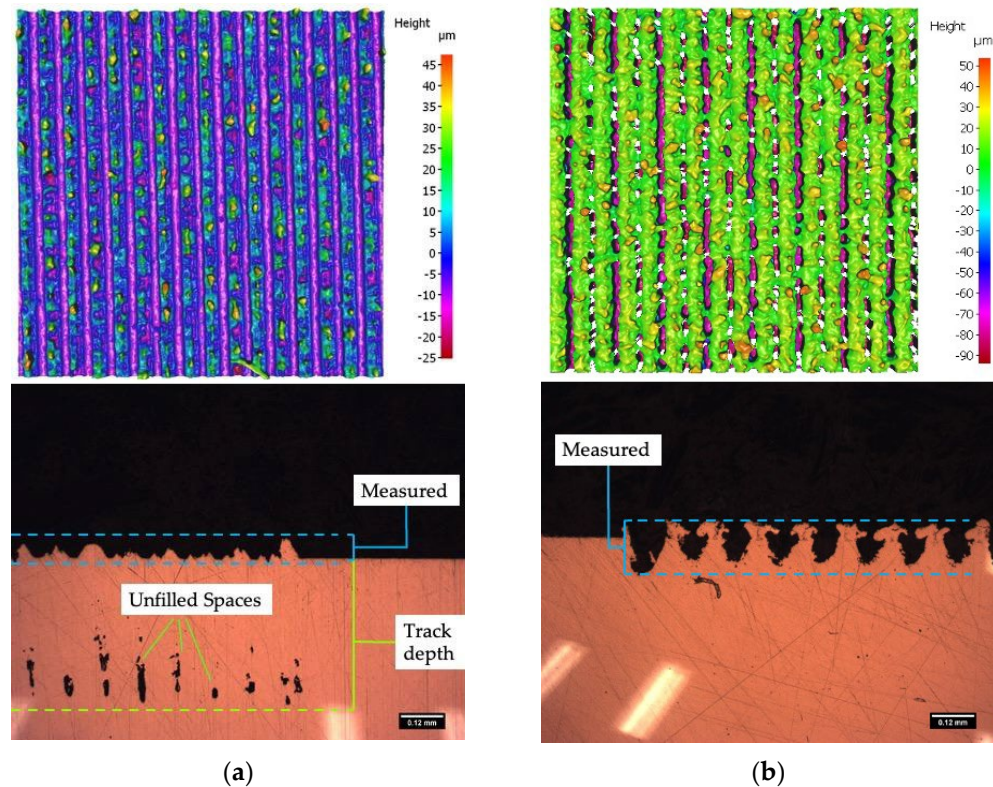


**Figure 5.** Surface mapping and cross section: (a)  $E_d = 35.37 \text{ J/cm}^2$  and  $V_s = 10 \text{ mm/s}$ ; (b)  $E_d = 35.37 \text{ J/cm}^2$  and  $V_s = 50 \text{ mm/s}$ .

Since a low  $V_s$  implies the laser beam spending more time in the same spot, the depth of the channel for  $V_s = 10 \text{ mm/s}$  is counterintuitive. Figure 5 shows the cross section of specimens at  $V_s = 10 \text{ mm/s}$  and  $V_s = 50 \text{ mm/s}$ . The low  $V_s$  sample shows an irregular surface, with poorly defined textures, and the presence of porosity in the lower part (Figure 5a). On the contrary, clearly defined textures with the expected shape (the hemispherical shape is due to the Gaussian profile of the laser beam) can be observed for the  $V_s = 50 \text{ mm/s}$  sample (Figure 5b).

These features are related to the material removal mechanism. The high amount of energy received by the surface when using a high energy density and a low scanning speed causes a melting of the material, which flattens the surface. The surface melting occurs due to the characteristics of the laser used. The predominant material removal mechanism with the use of nanosecond lasers is the heating-melting-vaporisation of the material, rather than the laser ablation mechanism typical of ultra-short pulse width lasers [24–26,56]. The porosity on the bottom of the textures indicates that the laser beam has reached this depth but the melting phenomenon has filled the engraved textures, due to the condensation and solidification of evaporated metal in small drops.

### 3.2. Micro-Hardness

Figure 6 shows the different values of surface micro-hardness measurements. For every case, the micro-hardness at the peak of the textures is significantly lower. Micro-hardness is reduced up to 33% in the texture area. As the measurements separates from

the surface, the micro-hardness tends to stabilise to the nominal value of the untextured AISI 630 (470 HV). Generally, 85% of the initial value is recovered at the bottom of the wear groove (40  $\mu\text{m}$ ).

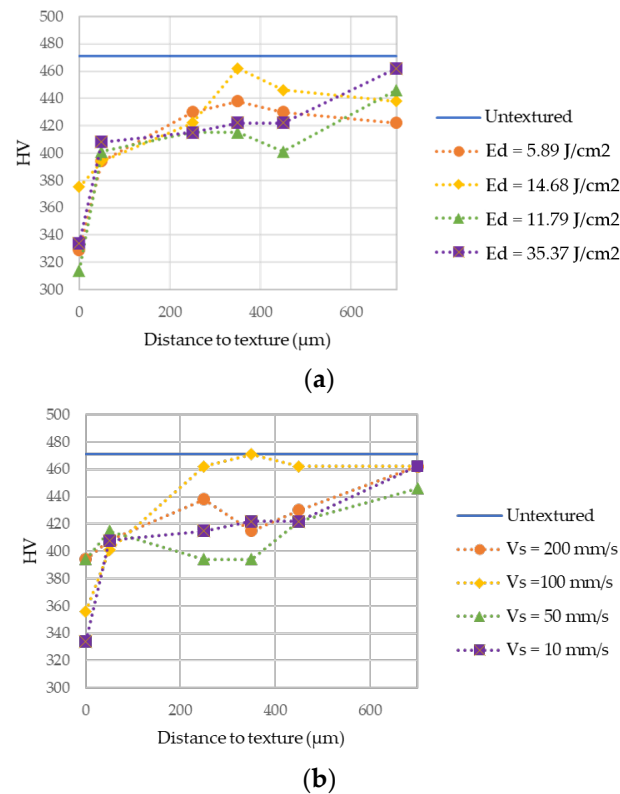


**Figure 6.** Micro-hardness: (a) At different  $E_d$  at fixed  $V_s = 10 \text{ mm/s}$ ; (b) At different  $V_s$  at fixed  $E_d = 35.37 \text{ J/cm}^2$ .

This significant decrease indicates that the laser treatment is softening the irradiated zone. This outcome is contrary to previous studies which have found a hardness increase in zones close to the texture, due to a martensitic transformation [57]. The loss of this martensitic transformation can therefore increase the friction coefficient and the wear rate, reducing the tribological performance of the surface. In addition, the reduction in hardness of the textured zone may be mainly due to the cooling effect of the vaporized material in the laser irradiation process. The particles of material released by the laser pulses do not solidify uniformly, affecting the microstructure and generating voids and micro-porosity in the modified layer that reduce the hardness of the material. Thus, no significant differences were found in the effect of  $E_d$  or  $V_s$ .

The initial microstructural condition of the 17-4 PH hardening steel is mainly constituted of martensite, corroborated after a chemical attack using a Fry reagent. Metallographic images were taken to ensure that no martensitic transformations have been reached. Since the  $E_d = 35.37 \text{ J/cm}^2$  and  $V_s = 10 \text{ mm/s}$  specimen has been submitted to the most aggressive LST parameters, it was compared with the untextured sample (Figure 7). As can be observed, the small layer identified for the untextured sample disappeared in the textured specimen. This reduction may be caused by the same phenomenon as the burr previously described. The melting process may decrease the mechanical properties of the surface, inducing some differences compared with the bulk material.

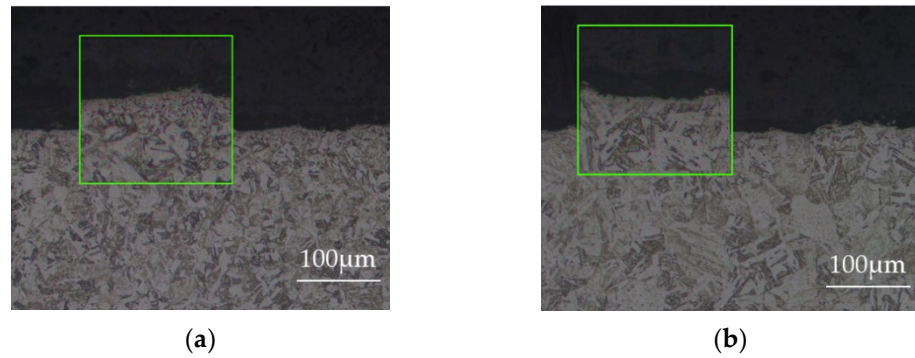


**Figure 7.** Microstructural analysis: (a) untextured sample; (b)  $E_d = 35.37 \text{ J/cm}^2$  and  $V_s = 10 \text{ mm/s}$  sample.

### 3.3. Friction Coefficient and Wear Behavior

The evolution of the friction coefficient is shown in Figure 8. Similarly, Figure 9 shows the average values of the friction coefficient as a function of the LST parameters.

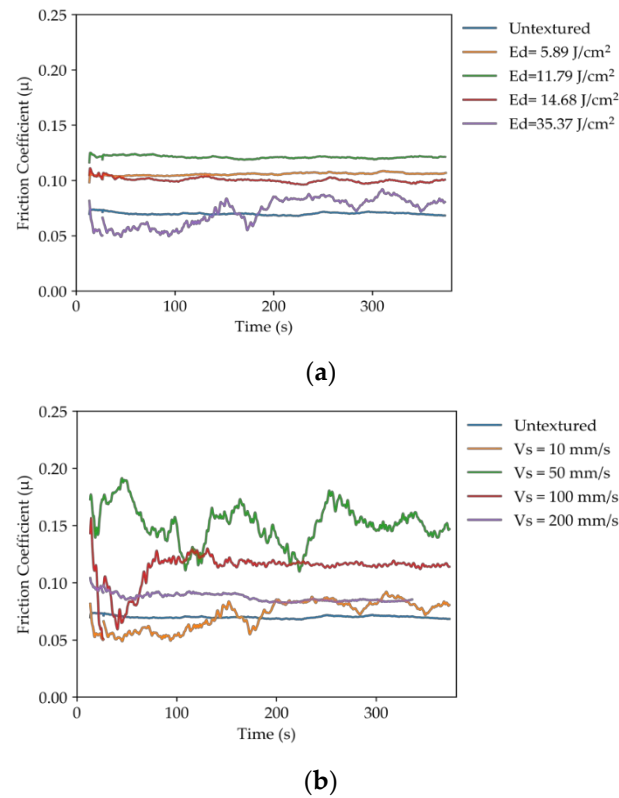


**Figure 8.** Friction coefficient as a function of (a)  $E_d$  ( $10 \text{ mm/s}$ ); (b)  $V_s$  ( $35.37 \text{ J/cm}^2$ ).

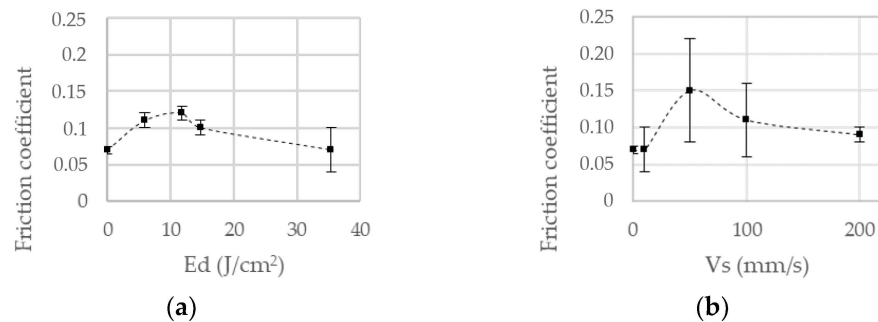


**Figure 9.** Friction coefficient average values: (a) For different  $E_d$  at fixed  $V_s = 10 \text{ mm/s}$ ; (b) For different  $V_s$  at fixed  $E_d = 35.37 \text{ J/cm}^2$ .

On the one hand, a stable behaviour for low  $V_s$  (10 mm/s) and medium and average  $E_d$  ( $<35.37$  J/cm<sup>2</sup>) samples is found. This can be associated with the low roughness values achieved in their LST processes. Nevertheless, the friction coefficient is increased by up to 200% for the  $E_d = 35.37$  J/cm<sup>2</sup> and  $V_s = 50$  mm/s samples. As was mentioned previously, this sample presents the higher  $S_{dr}$ . This fact combined with the aforementioned material softening, drastically increases the friction coefficient and the wear track depth.

On the other hand, high  $E_d$  (35.37 J/cm<sup>2</sup>) samples present a non-stable behaviour. The laser processing parameter combination ( $E_d = 35.37$  J/cm<sup>2</sup> and  $V_s = 50$  mm/s) shows the highest  $S_a$  roughness value of the textured specimens, as shown in Figure 3b. Under these conditions, the dimensions and shape of the asperities (shown in Figure 5b) causes a higher volume of wear debris during the friction test. These frictional debris are deposited on the sliding track, causing fluctuations in the coefficient of friction values. Under these conditions, the stick–slip phenomenon is clearly manifested, since the friction coefficient oscillates constantly between the static and the dynamic friction coefficient values. In this case, it was proven that the channels do not act as lubricant reservoirs but as stress concentrators. The textures locally decrease the thickness of the fluid layer, acting as barriers [42,43,58]. The presence of textures with a similar dimension to the contact area diameter might be another cause of the friction increase. Therefore, in this case the higher asperities make the sliding processes difficult, leading to the stick–slip phenomena, except for the  $E_d = 35.37$  J/cm<sup>2</sup> and  $V_s = 200$  mm/s sample, whose behavior is similar to the untextured sample. The behavior of the 35.37 J/cm<sup>2</sup> and  $V_s = 10$  mm/s sample is remarkable due to its reduced value up to 150 s. These sets of parameters decreased the friction coefficient compared with the untextured sample up to a limit, in which the abrasion of the channels diminished the reservoir effect.

This assumption is verified with the wear rate study presented in Figure 10, where the differences among initial and final weights (in grams, g) are represented (evaluated with a scale with  $10^{-4}$  g of resolution) vs.  $E_d$ .

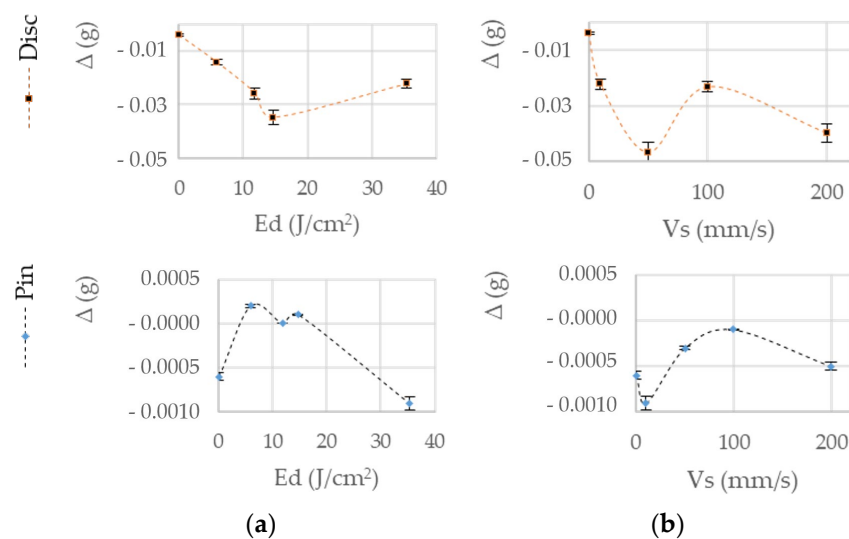


**Figure 10.** Wear rate based on weight variation for the disk and the pin: (a) For different  $E_d$  at fixed  $V_s = 10$  mm/s; (b) For different  $V_s$  at fixed  $E_d = 35.37$  J/cm<sup>2</sup>.

The main wear mechanism presented on the disc is abrasion (Figure 10b). Every sample, including the untextured one, reduces its weight after the friction tests. As expected, the maximum abrasion was found for 35.37 J/cm<sup>2</sup> and  $V_s = 50$  mm/s where the friction coefficient and the native surface were more irregular. In contrast, the main wear mechanism for the pin is adhesion (Figure 11a). Part of the disc material adhered to the pin surface, increasing its weight. Both wear mechanisms are enhanced by the material softening explained in the hardness results. Additionally, the breakage of the peaks of the

textures decreased the lubricant effect (Figure 11b), producing an increase in the friction coefficient values for high  $E_d$  parameters.

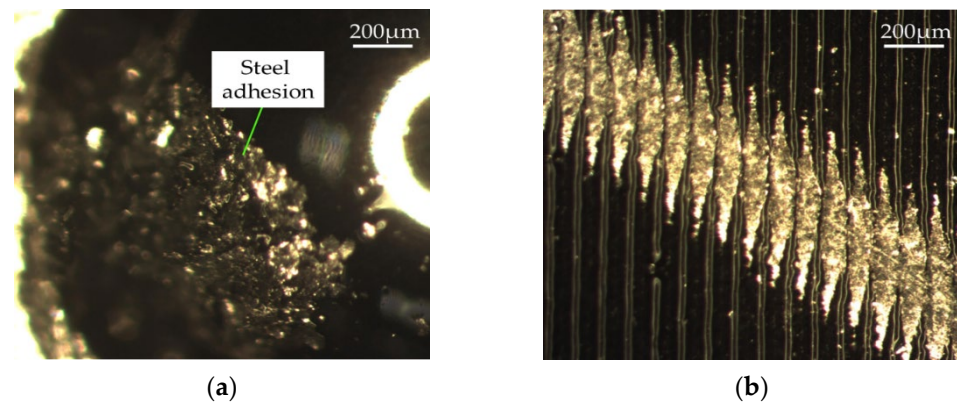


**Figure 11.** Stereoscopic macrographs: (a) Detail of the pin showing the steel adhesion; (b) Detail of the wear track obtained for  $35.37 \text{ J/cm}^2$  and  $V_s = 10 \text{ mm/s}$ .

A specific effect was observed on medium scale tracks from laser treatments. The cross-section of a textured specimen ( $35.37 \text{ J/cm}^2$ – $50 \text{ mm/s}$ ) subjected to the sliding test confirms that the development of medium scale textures can be used to trap the wear debris of the sliding process, as shown in Figure 12. This effect may help to reduce the third-body abrasive effect of sliding parts under friction conditions.

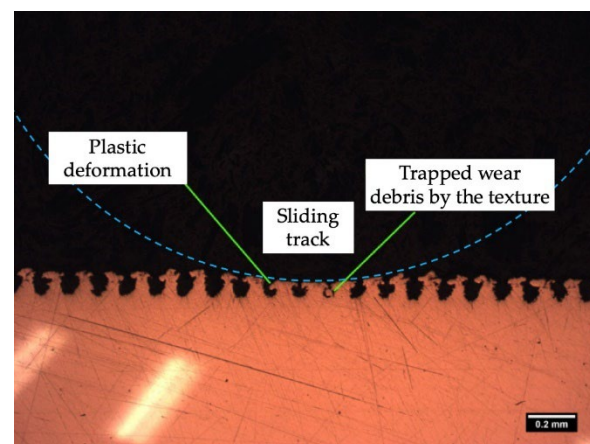


**Figure 12.** Wear debris trapped by the textured tracks.

#### 4. Conclusions

The present study has revealed that LST has a complex influence on the tribological behavior of surfaces. LST parameters modify the surface geometry of the textures.  $E_d$  linearly increases the depth of the channel, the  $S_a$ , and the  $S_{dr}$ . For the same parameters,  $V_s$  produces a peak value for  $50 \text{ mm/s}$ . However, profile roughness parameters present slight variations on the effect of LST parameters. Particularly,  $R_{Sm}$  has been found as an effective parameter to measure the width stability of the channel, which is affected by  $E_d$  due to the melting mechanism of LST. This melting mechanism also affects the real depth of the channels for low  $V_s$  ( $10 \text{ mm/s}$ ) producing pores on the bottom of the surface.

Surface integrity is modified by reducing the micro-hardness up to 33% on the heat-affected zone. Nevertheless, 85% of the bulk micro-hardness is recovered at  $40 \mu\text{m}$ . This micro-hardness drop is due to a softening of the material. An increase in the instability of the friction coefficient was detected for high  $E_d$ , caused by the roughness increase and the softening of the material. Finally, the wear mechanisms were identified. Pin presented mainly steel adhesion and disc abrasion. The abrasion of the disc removed the effect of the channels, reducing its efficiency regarding lubricant retention.

To summarize, the integration of the surfaces depends on multiple factors and the formulation of mathematical models relating to the variables of interest may be a future work.

**Author Contributions:** Conceptualization, J.S. and J.M.V.-M.; Methodology, G.D. and M.B.; Formal analysis, G.D. and I.D.S. Resources, J.S.; Writing—original draft preparation, G.D., J.S., J.M.V.-M. and I.D.S.; Writing—review and editing, J.S., J.M.V.-M., I.D.S. and M.B.; Supervision, J.S. and J.M.V.-M. All authors have read and agreed to the published version of the manuscript.

**Funding:** This work has received financial support from the Spanish Government (MINECO/AEI/FEDER, No. DPI2017-84935-R and EQC2019-005674-P).

**Institutional Review Board Statement:** Not applicable.

**Informed Consent Statement:** Not applicable.

**Data Availability Statement:** Not applicable.

**Acknowledgments:** Authors want to acknowledge the company Titania for the support provided in the metallographic characterization of AISI 630.

**Conflicts of Interest:** The authors declare no conflict of interest.

## References

1. Mang, T.; Bobzin, K.; Bartels, T. *Industrial Tribology*, 1st ed.; Wiley-VCH Verlag & Co.: Weinheim, Germany, 2010; pp. 1–6.
2. Hutchings, I.; Shipway, P. 3-Friction. In *Tribology: Friction and Wear of Engineering Materials*, 2nd ed.; Hutchings, I., Shipway, P., Eds.; Elsevier: Amsterdam, The Netherlands, 2017; pp. 37–77.
3. Stachowiak, G.W.; Batchelor, A.W. *Engineering Tribology*, 4th ed.; Elsevier: Amsterdam, The Netherlands, 2005; pp. 357–504.
4. Bowden, F.P.; Tabor, D. *The Friction and Lubrication of Solids*, 2nd ed.; Oxford University Press: New York, NY, USA, 1964; Volume 1, pp. 1–366.
5. M’Ndange-Pfupfu, A.; Marks, L.D. A Dislocation-Based Analytical Model for the Nanoscale Processes of Shear and Plowing Friction. *Tribol. Lett.* **2010**, *39*, 163–167. [[CrossRef](#)]
6. Braun, O.M.; Naumovets, A.G. Nanotribology: Microscopic Mechanisms of Friction. *Surf. Sci. Rep.* **2006**, *60*, 79–158. [[CrossRef](#)]
7. Hu, Y.; Ma, T.; Wang, H. Energy Dissipation in Atomic-Scale Friction. *Friction* **2013**, *1*, 24–40. [[CrossRef](#)]
8. Kumar Sharma, A.; Kumar Tiwari, A.; Dixit, A.R. Effects of Minimum Quantity Lubrication (MQL) in Machining Processes Using Conventional and Nanofluid Based Cutting Fluids: A Comprehensive Review. *J. Clean. Prod.* **2016**, *127*, 1–18. [[CrossRef](#)]
9. Gropper, D.; Wang, L.; Harvey, T.J. Hydrodynamic Lubrication of Textured Surfaces: A Review of Modeling Techniques and Key Findings. *Tribol. Int.* **2016**, *94*, 509–529. [[CrossRef](#)]
10. Wang, Q.J.; Chung, Y.-W. *Encyclopedia of Tribology*, 1st ed.; Springer: Boston, MA, USA, 2013; pp. 1422–1537.
11. Hsu, S.M.; Jing, Y.; Hua, D.; Zhang, H. Friction Reduction Using Discrete Surface Textures: Principle and Design. *J. Phys. D Appl. Phys.* **2014**, *47*, 335307. [[CrossRef](#)]
12. Lu, X.; Khonsari, M.M. An Experimental Investigation of Dimple Effect on the Stribeck Curve of Journal Bearings. *Tribol. Lett.* **2007**, *27*, 169–176. [[CrossRef](#)]
13. Vladescu, S.C.; Olver, A.V.; Pegg, I.G.; Reddyhoff, T. The Effects of Surface Texture in Reciprocating Contacts—An Experimental Study. *Tribol. Int.* **2015**, *82*, 28–42. [[CrossRef](#)]
14. Vlădescu, S.-C.; Olver, A.V.; Pegg, I.G.; Reddyhoff, T. Combined Friction and Wear Reduction in a Reciprocating Contact through Laser Surface Texturing. *Wear* **2016**, *358–359*, 51–61. [[CrossRef](#)]
15. Sedlaček, M.; Guštin, A.Z.; Žužek, B. Influence of Laser Surface Texturing Sequence on Fatigue Properties of Coated Cold Work Tool Steel. *Metals* **2020**, *10*, 1636. [[CrossRef](#)]
16. Gachot, C.; Rosenkranz, A.; Hsu, S.M.; Costa, H.L. A Critical Assessment of Surface Texturing for Friction and Wear Improvement. *Wear* **2017**, *372–373*, 21–41. [[CrossRef](#)]
17. Etsion, I. Improving Tribological Performance of Mechanical Components by Laser Surface Texturing. *Tribol. Lett.* **2004**, *17*, 733–737. [[CrossRef](#)]
18. Marchetto, D.; Rota, A.; Calabri, L.; Gazzadi, G.C.; Menozzi, C.; Valeri, S. AFM Investigation of Tribological Properties of Nano-Patterned Silicon Surface. *Wear* **2008**, *265*, 577–582. [[CrossRef](#)]
19. Chen, L.; Liu, Z.; Shen, Q. Enhancing Tribological Performance by Anodizing Micro-Textured Surfaces with Nano-MoS<sub>2</sub> Coatings Prepared on Aluminum-Silicon Alloys. *Tribol. Int.* **2018**, *122*, 84–95. [[CrossRef](#)]
20. Yamaguchi, K.; Takada, Y.; Tsukuda, Y.; Ota, M.; Egashira, K.; Morita, T. Friction Characteristics of Textured Surface Created by Electrical Discharge Machining under Lubrication. *Procedia CIRP* **2016**, *42*, 662–667. [[CrossRef](#)]
21. Walker, J.C.; Kamps, T.J.; Lam, J.W.; Mitchell-Smith, J.; Clare, A.T. Tribological Behaviour of an Electrochemical Jet Machined Textured Al-Si Automotive Cylinder Liner Material. *Wear* **2017**, *376–377*, 1611–1621. [[CrossRef](#)]
22. Walter, K.M.; van de Vorst, B.; Hessel, M.B.; Nico, K.M. Design for Rapid Manufacturing Functional SLS Parts. In Proceedings of the 2nd I\*PROMS Virtual International Conference, Eindhoven, The Netherlands, 13–14 July 2006.

23. El-Hofy, H.A. *Fundamentals of Machining Processes: Conventional and Nonconventional Processes*, 3rd ed.; CRC Press: Boca Raton, FL, USA, 2014; pp. 400–406.
24. Bhattacharyya, B.; Doloi, B. (Eds.) Machining Processes Utilizing Thermal Energy. In *Modern Machining Technology: Advanced, Hybrid, Micro Machining and Super Finishing Technology*, 1st ed.; Academic Press: London, UK, 2020; pp. 131–363.
25. Bhattacharyya, B.; Doloi, B. (Eds.) Micromachining Processes. In *Modern Machining Technology: Advanced, Hybrid, Micro Machining and Super Finishing Technology*, 1st ed.; Academic Press: London, UK, 2020; pp. 593–673.
26. Mishra, S.; Yadava, V. Laser Beam MicroMachining (LBMM)—A Review. *Opt. Lasers Eng.* **2015**, *73*, 89–122. [[CrossRef](#)]
27. Yuan, L.; Lin, N.; Wang, W.; Zhang, H.; Liu, Z.; Yu, Y.; Zeng, Q.; Wu, Y. Correlation between surface textural parameter and tribological behaviour of four metal materials with laser surface texturing (LST). *Appl. Surf. Sci.* **2022**, *583*, 152410. [[CrossRef](#)]
28. Salguero, J.; Del Sol, I.; Vazquez-Martinez, J.M.; Schertzer, M.J.; Iglesias, P. Effect of laser parameters on the tribological behavior of Ti6Al4V titanium microtextures under lubricated conditions. *Wear* **2019**, *426–427*, 1272–1279. [[CrossRef](#)]
29. Mang, T.; Dresel, W. *Lubricants and Lubrication*, 3rd ed.; Wiley-VCH Verlag & Co.: Weinheim, Germany, 2007; pp. 11–30.
30. Pawlus, P.; Galda, L.; Dzierwa, A.; Koszela, W. Abrasive Wear Resistance of Textured Steel Rings. *Wear* **2009**, *267*, 1873–1882. [[CrossRef](#)]
31. Yu, H.; Xiaolei, A.E.; Ae, W.; Zhou, F. Geometric Shape Effects of Surface Texture on the Generation of Hydrodynamic Pressure between Conformal Contacting Surfaces. *Tribol. Lett.* **2010**, *37*, 123–130. [[CrossRef](#)]
32. Sedláček, M.; Podgornik, B.; Ramalho, A.; Česnik, D. Influence of Geometry and the Sequence of Surface Texturing Process on Tribological Properties. *Tribol. Int.* **2017**, *115*, 268–273. [[CrossRef](#)]
33. Galda, L.; Pawlus, P.; Sep, J. Dimples Shape and Distribution Effect on Characteristics of Stribeck Curve. *Tribol. Int.* **2009**, *42*, 1505–1512. [[CrossRef](#)]
34. Schneider, J.; Braun, D.; Greiner, C. Laser Textured Surfaces for Mixed Lubrication: Influence of Aspect Ratio, Textured Area and Dimple Arrangement. *Lubricants* **2017**, *5*, 32. [[CrossRef](#)]
35. Wang, Z.; Li, Y.B.; Bai, F.; Wang, C.W.; Zhao, Q.Z. Angle-Dependent Lubricated Tribological Properties of Stainless Steel by Femtosecond Laser Surface Texturing. *Opt. Laser Technol.* **2016**, *81*, 60–66. [[CrossRef](#)]
36. Shimizu, T.; Kobayashi, H.; Vorholt, J.; Yang, M. Lubrication Analysis of Micro-Dimple Textured Die Surface by Direct Observation of Contact Interface in Sheet Metal Forming. *Metals* **2019**, *9*, 917. [[CrossRef](#)]
37. Boidi, G.; Tertuliano, I.S.; Profito, F.J.; de Rossi, W.; Machado, I.F. Effect of Laser Surface Texturing on Friction Behaviour in Elastohydrodynamically Lubricated Point Contacts under Different Sliding-Rolling Conditions. *Tribol. Int.* **2020**, *149*, 105613. [[CrossRef](#)]
38. Rosenkranz, A.; Szurdak, A.; Grützmacher, P.G.; Hirt, G.; Mücklich, F. Friction Reduction Induced by Elliptical Surface Patterns under Lubricated Conditions. *Adv. Eng. Mater.* **2018**, *20*, 1700731. [[CrossRef](#)]
39. Vilhena, L.M.; Podgornik, B.; Vižintin, J.; Možina, J. Influence of Texturing Parameters and Contact Conditions on Tribological Behaviour of Laser Textured Surfaces. *Meccanica* **2011**, *46*, 567–575. [[CrossRef](#)]
40. Braun, D.; Greiner, C.; Schneider, J.; Gumbsch, P. Efficiency of Laser Surface Texturing in the Reduction of Friction under Mixed Lubrication. *Tribol. Int.* **2014**, *77*, 142–147. [[CrossRef](#)]
41. Greiner, C.; Schäfer, M.; Popp, U.; Gumbsch, P. Contact Splitting and the Effect of Dimple Depth on Static Friction of Textured Surfaces. *ACS Appl. Mater.* **2014**, *6*, 7986–7990. [[CrossRef](#)] [[PubMed](#)]
42. Costa, H.L.; Hutchings, I.M. Hydrodynamic Lubrication of Textured Steel Surfaces under Reciprocating Sliding Conditions. *Tribol. Int.* **2007**, *40*, 1227–1238. [[CrossRef](#)]
43. Kovalchenko, A.; Ajayi, O.; Erdemir, A.; Fenske, G. Friction and wear behavior of laser textured surface under lubricated initial point contact. *Wear* **2011**, *271*, 1719–1725. [[CrossRef](#)]
44. Bracco, G.; Holst, B. *Surface Science Techniques*, 1st ed.; Springer: Berlin, Germany, 2013; pp. 3–34.
45. Drelich, J.; Chibowski, E.; Meng, D.D.; Terpilowski, K. Hydrophilic and Superhydrophilic Surfaces and Materials. *Soft Matter* **2011**, *7*, 9804–9828. [[CrossRef](#)]
46. Biolin Scientific. Technical Note. Influence of Surface Roughness on Contact Angle and Wettability. Available online: <https://cdn2.hubspot.net/hubfs/516902/Pdf/Attension/Tech%20Notes/AT-TN-07-Surface-roughness-CA-wettability.pdf> (accessed on 25 February 2022).
47. Wojciechowski, L.; Kubiak, K.J.; Mathia, T.G. Roughness and Wettability of Surfaces in Boundary Lubricated Scuffing Wear. *Tribol. Int.* **2016**, *93*, 593–601. [[CrossRef](#)]
48. Kubiak, K.J.; Wilson, M.C.T.; Mathia, T.G.; Carval, P. Wettability versus Roughness of Engineering Surfaces. *Wear* **2011**, *271*, 523–528. [[CrossRef](#)]
49. Ahuir-Torres, J.L.; Arenas, M.A.; Perrie, W.; Dearden, G.; de Damborenea, J. Surface Texturing of Aluminium Alloy AA2024-T3 by Picosecond Laser: Effect on Wettability and Corrosion Properties. *Surf. Coat. Technol.* **2017**, *321*, 279–291. [[CrossRef](#)]
50. Guimarães, B.; Fernandes, C.M.; Figueiredo, D.; Carvalho, O.; Silva, F.S.; Miranda, G. Effect of Laser Surface Texturing on the Wettability of WC-Co Cutting Tools. *Int. J. Adv. Manuf. Technol.* **2020**, *111*, 1991–1999. [[CrossRef](#)]
51. Genna, S.; Giannini, O.; Guarino, S.; Ponticelli, G.S.; Tagliaferri, F. Laser Texturing of AISI 304 Stainless Steel: Experimental Analysis and Genetic Algorithm Optimisation to Control the Surface Wettability. *Int. J. Adv. Manuf. Technol.* **2020**, *110*, 3005–3022. [[CrossRef](#)]

52. Vazquez-Martínez, J.M.; Salguero, J.; Mayuet, P.F.; Fernandez-Vidal, S.R.; Batista, M. Effects of Laser Microtexturing on the Wetting Behavior of Ti6Al4V Alloy. *Coatings* **2018**, *8*, 145. [[CrossRef](#)]
53. ASTM International. Standard Test Method for Wear Testing with a Pin-on-Disk Apparatus G99-17. In *Annual Book of ASTM Standards*; ASTM International: West Conshohocken, PA, USA, 2017; Volume 5, pp. 1–6.
54. AK Steel 17-4 PH®Precipitation Hardening Stainless Steel, Condition H 900. Available online: <http://www.matweb.com/search/datasheet.aspx?MatGUID=ef0844b850954281a438dc76c1e0b49e> (accessed on 25 February 2022).
55. International Standard Organization (ISO). *Geometrical Product Specifications (GPS)-Surface Texture: Profile Method-Rules and Procedures for the Assessment of Surface Texture (ISO 4288)*; International Standard Organization: Geneva, Switzerland, 1999.
56. Piqué, A.; Chrisey, D.B.; Paul Christensen, C. Laser Direct-Write Micromachining. In *Direct-Write Technologies for Rapid Prototyping*, 1st ed.; Piqué, A., Ed.; Academic Press: London, UK, 2002; pp. 385–414.
57. Vazquez-Martínez, J.M.; Salguero, J.; Blanco, E.; González-Leal, J.M. Nanosecond Pulsed Laser Irradiation of Titanium Alloy Substrate: Effects of Periodic Patterned Topography on the Optical Properties of Colorizing Surfaces. *Coatings* **2019**, *9*, 658. [[CrossRef](#)]
58. Kovalchenko, A.; Ajayi, O.; Erdemir, A.; Fenske, G.; Etsion, I. The Effect of Laser Surface Texturing on Transitions in Lubrication Regimes during Unidirectional Sliding Contact. *Tribol. Int.* **2005**, *38*, 219–225. [[CrossRef](#)]